JOURNAL OF GUIDANCE, CONTROL, AND DYNAMICS
Vol. 28, No. 2, March–April 2005

Time- and Phase-Space Stability Analysis of the Jupiter–Sun System

D. G. Tuckness
University of Oklahoma, Norman, Oklahoma 73019-1052

A comparison of dynamic stability determination for a celestial body is made between the Newtonian time domain and the phase-space domain. A new method of using the line of syzygies for determination of the stability of a third body moving in the region of two primary bodies is reviewed for accuracy via more proven or investigated phase-space methods such as Poincaré phase space surface of section methods. Phase-space surface of section methods appear to verify that the use of the line of syzygies as a stability criteria is valid, shedding new information of the stable motion of the third body, especially in the time domain.

Nomenclature

C = Jacobin constant of integration
F_{Q1} = $\partial F/\partial Q_1$
F_{Q2} = $\partial F/\partial Q_2$
H = Hamiltonian constant of integration
L_4 = Lagrange point
M_1 = mass of primary
M_2 = mass of secondary
P_1 = Hamiltonian x momenta
P_2 = Hamiltonian y momenta
Q_1 = Hamiltonian x axis
Q_2 = Hamiltonian y axis
R_1 = radial distance to primary M_1
R_2 = radial distance to secondary M_2
X = sidereal or nonrotating x axis
x = rotating x value in time domain
Y = sidereal or nonrotating y axis
y = rotating y value in time domain
θ = initial direction of third body motion from L_4
μ = gravitational parameter
Ω_x = $\partial\Omega/\partial x$
Ω_y = $\partial\Omega/\partial y$

Introduction

MANY researchers, such as Hénon,[1,2] Henon and Hiles,[3] and Poincaré,[4] among others, have studied the long-term stability of dynamic systems utilizing Hamiltonian phase-space (frequency-domain) methods such as surface-of-section mappings. Other researchers, such as Alfriend,[5] Deprit,[6] Henrard,[7] Pederson,[8] Szebehely,[9] and Tuckness[10] have studied long-term stability of dynamic systems using a Newtonian time-domain approach. Both domain studies (phase and time) have advantages and disadvantages. The phase-space domain pseudo removes time from the problem, offering the ability to study long- (possibly infinite-) term stability without time constraints. However, because it is a Hamiltonian phase-space representation, it is somewhat more difficult to apply the findings to the everyday Newtonian time-domain world. An advantage of time-domain analysis is the ease of interpreting the resulting data and not requiring a Hamiltonian constant. However, the disadvantage of time-domain analysis surfaces in the difficult attempt to investigate the system for an infinite time. These two different approaches are investigated and compared in this paper to study the long-term stability of a dynamic system. The dynamic system investigated is the circular restricted problem of three bodies as will be explained.

Szebehely,[9] Tuckness,[10] and McKenzie and Szebehely[11] have had success in studying the dynamic stability of the three-body system using a Newtonian time-domain boundary envelope approach. The boundary envelope approach is a method of bounding the kinetic energy of the third body as it departs (or passes through) the L_4 point. This study compares this Newtonian time-domain boundary envelope measure, or interpretation, of stability to the classical Poincaré surface of section interpretation found using phase-space investigative techniques. Both methods are used to investigate the motion of a third body for stability in the same Jupiter–sun system. This study compares the phase-space-domain results with the time-domain results applied to the stability of a third body in motion near one of the equilibrium points, the L_4 Lagrange point. In particular, it is shown that the time-domain boundary envelope approach used as a stability measure in Refs. 9–11 offers very similar and yet totally independent results compared to the traditional phase-space methods. Furthermore, the boundary envelope approach presents the stability criteria in a time domain Cartesian coordinate system, which can be easier to interpret for real-time application and analysis. It is also shown that the time-domain studies can be used to better understand the results of the phase-space studies that can sometimes be difficult to analyze.

Introduction to the System Under Investigation

The system under investigation is the motion of a third body under the influence of the gravitational pull of the sun and Jupiter ($\mu = 0.000953875$ dimensionless units). A brief description of the model of the circular restricted three-body problem representing time-domain motion of the third body is as follows: Two bodies revolve around their center of mass in circular orbits under the influence of their mutual gravitational attraction. A third body (influenced by the previous two but not influencing their motion) moves

D. G. Tuckness is professor of aerospace and mechanical engineering at the University of Oklahoma. He received a B.S. in physics and mathematics (double major) from Southeastern Oklahoma State University, 1981, a M.S. in aerospace engineering from the University of Texas at Austin, 1985, and a Ph.D. in aerospace engineering from the University of Texas at Austin, 1988. Before joining the aerospace and mechanical engineering faculty at the University of Oklahoma, he served as the associate chairman of mechanical and aerospace engineering and as the director of aerospace engineering program at the University of Texas at Arlington. His research interests include spacecraft/mission analysis and design, astrodynamics and atmospheric flight dynamics, statistical estimation theory, and guidance and navigation systems. He is an Associate Fellow of AIAA.

Received 4 June 2003; revision received 12 November 2003; accepted for publication 14 November 2003.

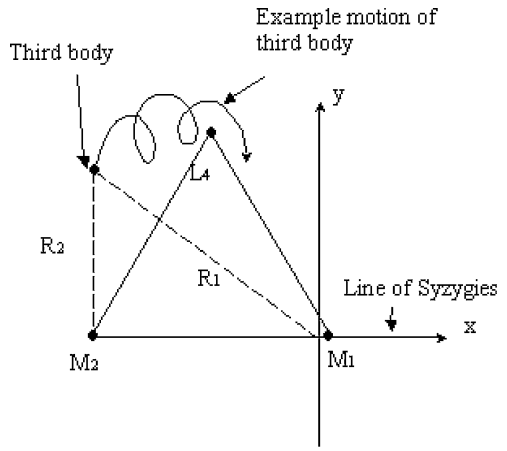

Fig. 1 Restricted problem of third body.

in the plane defined by the two revolving bodies. For additional details pertaining to the structure of the circular restricted problem of three bodies see Szebehely.[9]

The equations that describe the motion of the third body are

$$\ddot{x} - 2\dot{y} = \Omega_x \tag{1}$$

$$\ddot{y} + 2\dot{x} = \Omega_y \tag{2}$$

where the dot represents the time derivative. Also

$$\Omega = (1-\mu)\left[R_1^2/2 + 1/R_1\right] + \mu\left[R_2^2/2 + 1/R_2\right] \tag{3}$$

where

$$R_1^2 = (x-\mu)^2 + y^2 \tag{4}$$

$$R_2^2 = (x+\mu-1)^2 + y^2 \tag{5}$$

The Jacobian integral is

$$\dot{x}^2 + \dot{y}^2 = 2\Omega - C \tag{6}$$

The return to the fixed system (dimensionless sidereal) is performed using the transformation

$$X = x\cos t - y\sin t \tag{7}$$

$$Y = x\sin t + y\cos t \tag{8}$$

where X and Y are the dimensionless sidereal coordinates.

Figure 1 shows the basic orientation of the third body in the xy plane. When the Newtonian third-body equations of motion [Eqs. (1) and (2)] are used, the librational motion of the third motion is numerically integrated using a classical eighth-order Runge–Kutta integrator with a seventh order for automatic step size control allowing an error no greater than 1×10^{-10} in C, the Jacobian constant of integration calculated from Eq. (6).

Construction of the Time-Domain Boundary Envelopes

By the numerical integration of the third-body equations of motion [Eqs. (1) and (2)], a set of boundary envelopes are formulated by Tuckness.[10] The boundary envelopes bound the allowed initial velocities (kinetic energies) or pass through velocities a third body is permitted to have at the L_4 point. That is, if a third body starts its motion or passes through the L_4 point with a velocity greater than what the boundary envelope permits, then it is classified unstable. Tuckness [10] defines unstable motion as third-body motion that crosses the line of syzygies (x axis) within a defined time frame. The defined time frame in this study is selected to be 5,000,000 dimensionless time units, equivalent to approximately 31,416,000 years for the Jupiter–sun system.

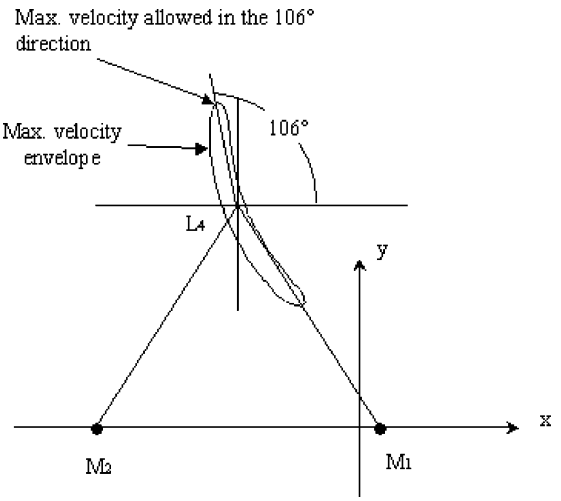

Fig. 2 Construction of the boundary envelope.

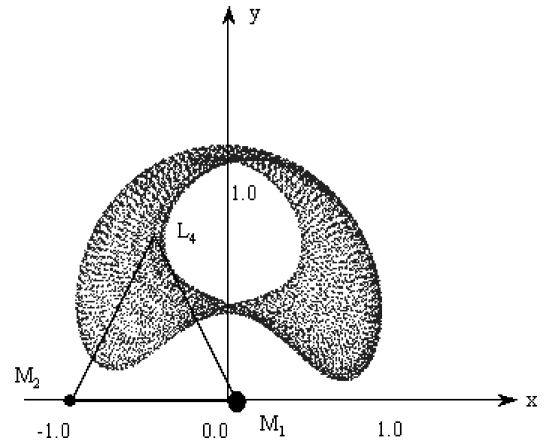

Fig. 3 Stable librational motion.

Again, the boundary envelopes formulated by Tuckness[10] are found by determining the initial conditions with which a third body could start or pass through at L_4, in a specified direction, such that its librational motion does not cross the x axisto within a 5,000,000 time unit limit. For example, the maximum velocity in the 106-deg direction shown in Fig. 2 is found by starting the third body at L_4 with a very large velocity, integrating its trajectory for 5,000,000 time units, and checking to see if the third body crosses the x axis (line of syzygies) before reaching the numerical integration stopping time of 5,000,000 time units. If the third body crosses the x axis before reaching the numerical integration stopping time of 5,000,000 time units, the initial velocity of the third body is decreased by 0.00001 dimensionless velocity units and the whole procedure repeated. This continues until a maximum velocity is found that allows the third body to librate around L_4 for the full 5,000,000 time units without crossing the x axis. Figure 3 shows a stable-type librational motion, that is, the third body did not cross the line of syzygies (x axis) in the specified time interval. This procedure is performed for the full 360 deg surrounding L_4.

Determining the maximum velocity allowed in a single direction constitutes a velocity vector with magnitude and direction. Connecting the maximum velocity vector endpoints together for the full 360 deg surrounding L_4 forms the maximum velocity envelope as shown in Fig. 4.

This approach is first introduced by McKenzie and Szebehely.[11] In their paper, they do not allow motion of the third body to cross the x axis, thus establishing their stability criteria boundary as the x axis. Tuckness[10] performed an in-depth investigation of implementing the x axis as a stability criterion and investigated various time limits of integration and various values of μ. Tuckness found that using the

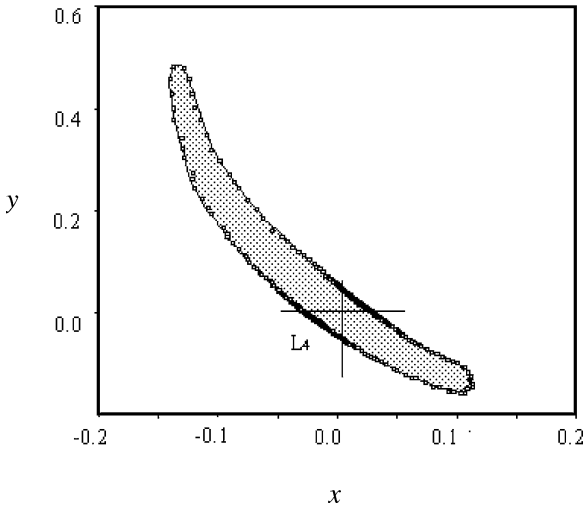

Fig. 4 Example velocity boundary envelope.

x axis as a stability criterion is valid for a wide range in values of μ.

One point from this boundary envelope, the maximum velocity of the 106-deg direction, is initially selected for comparison to the results found using Hamiltonian phase-space stability determination methods. Other points are additionally investigated and show similar comparisons between the time and phase-space domains that are discussed later in this study.

Hamiltonian Phase Space Description of the Three-Body System

To analyze the three-body stability in the phase-space domain, a quadratic area-preserving mapping is used to transform the Newtonian time-domain equations of motion (1) and (2) to a Hamiltonian system. In the transformation of the Newtonian equations of motion to the Hamiltonian equations, the following system of equations are found:

$$Q_1 = x \tag{9}$$

$$Q_2 = y \tag{10}$$

with momenta

$$P_1 = \dot{x} - y \tag{11}$$

$$P_2 = \dot{y} + x \tag{12}$$

Now, the time rates of change of the phase space variables are

$$\dot{Q}_1 = P_1 + Q_2 \tag{13}$$

$$\dot{Q}_2 = P_2 + Q_1 \tag{14}$$

$$\dot{P}_1 = P_2 + F_{Q1} \tag{15}$$

$$\dot{P}_2 = -P_1 + F_{Q2} \tag{16}$$

with the forcing function described as

$$F = \frac{1-\mu}{\sqrt{(Q_1-\mu)^2 + Q_2^2}} + \frac{\mu}{\sqrt{(Q_1+1-\mu)^2 + Q_2^2}} \tag{17}$$

Equations (13–16) are known as the Hamiltonian equations and are accompanied with a constant of integration called the Hamiltonian, H,

$$H = \frac{1}{2}\left(P_1^2 + P_2^2\right) + (Q_2 P_1 - Q_1 P_2) - \left[\frac{1-\mu}{\sqrt{(Q_1-\mu)^2 + Q_2^2}} + \frac{\mu}{\sqrt{(Q_1+1-\mu)^2 + Q_2^2}}\right] \tag{18}$$

Surface of Section

The third-body equations of motion are expressed in Hamiltonian form [Eqs. (15) and (16)], are numerically integrated for 5,000,000 time units using the same Runge–Kutta $\frac{7}{8}$ numerical integrator described in the Newtonian time-domain studies described earlier. Again no error greater than 1×10^{-10} is permitted in the constant of integration H calculated from Eq. (18).

Now, visualizing periodic trajectories in the Newtonian time domain is, for the most part, not very difficult, but when motion becomes quasi periodic or chaotic it is easier to use a Poincaré surface of section to analyze the stability. A surface of section is constructed by first defining a hyperplane in the phase space and then plotting selected Hamiltonian trajectory coordinates whenever the third body pierces the hyperplane. Formally, Poincaré surface of sections for the three-body problem are briefly described as follows: A solution of the Hamiltonian equations of motion [Eqs. (15) and (16)] can be represented as a trajectory in a four-dimensional phase space**.** Because of the existence of the integral of motion, H in Eq. (18), the trajectory lies in a three-dimensional subspace H that is equal to a constant of the phase space. Therefore, given H, a point of the trajectory can be defined by three coordinates only, for example, x, y, and $\dot{x}$. The value of the missing coordinate is found from Eq. (18). Thus, it is sufficient to represent the trajectory in a three-dimensional space (x, y, and $\dot{x}$). Now, consider the successive intersections of this three-dimensional trajectory with a two-dimensional surface, which is called the surface of section. Select the hyperplane, or two-dimensional surface, $y = \sqrt{3}/2$, and consider only the intersections in the positive $\dot{y}$ direction, that is, with $\dot{y}$ greater than zero; the four-dimensional trajectory is now represented by a set of points in the $(x, \dot{x})$ or (Q_1, P_1) plane, and the results can be represented in a much more compact manner. Here $y = \sqrt{3}/2$ is chosen because having a surface that passes through the point of origin L_4 results in all motion intersecting the surface. Thus, all stable motion is represented in the phase plot. Figure 5 shows the process that forms the surface of section. There is no serious loss of information because the most interesting properties of the trajectory are reflected into corresponding properties of the set of points.

The trajectory information in the phase space can basically be divided into three distinct regions or significant types of motion for the quadratic area-preserving surface of section mapping. One region contains primarily stable trajectories, trajectories originating from elliptic points that result in regular motion on invariant curves around the fixed points of stable periodic orbits. This first stable region is connected to a second region, made up of mostly singular points (hyperbolic points) which, when combined, are called a separatrix. In general the separatrix separates the motion around the first region of stable elliptic points from a third region that consists of irregular, stochastic trajectories and in general represents unstable motion.

Of particular importance in this study is the area of the plot that seperates stable motion from unstable motion, the separatrix.

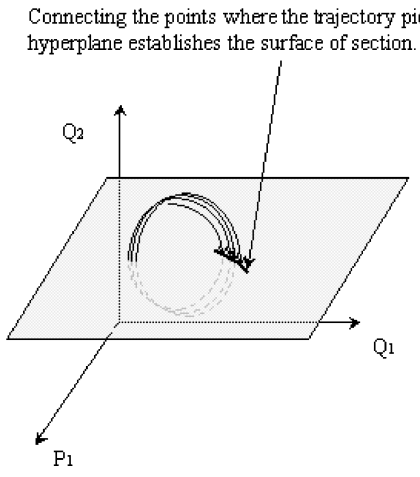

Fig. 5 Construction of the surface of section.

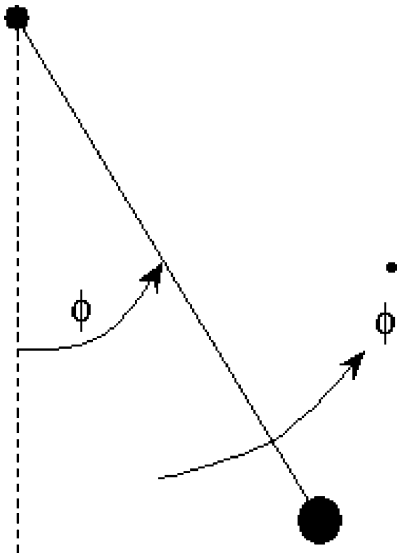

Fig. 6 Simple swinging pendulum.

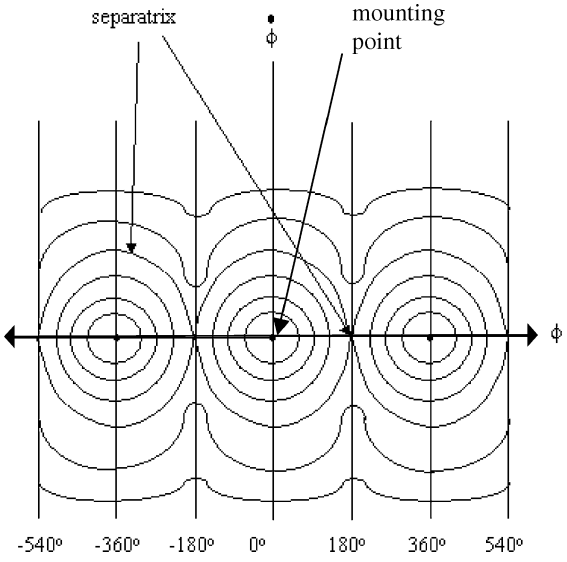

Fig. 7 Phase plot of simple swinging pendulum.

A simple example of the information that the separatrix contains is shown with the following example of a simple swinging pendulum.

For small energies, the pendulum performs oscillatory motion in the form of swinging motion about the equilibrium point ϕ and $\dot{\phi} = 0$ (Fig. 6). Creating a phase portrait by plotting ϕ vs $\dot{\phi}$ results in a set of curves centered about the equilibrium point. As the energy increases, the pendulum performs larger and larger swinging motions (librations) until a point is reached when the pendulum swing starts to perform rotational motion about the mounting point. A critical point is reached when the pendulum has enough energy to swing all of the way from $\phi = 0$ to $\phi = 180$ deg. The point at $\phi = 180$ deg is a dividing point between stable motion (actual swinging motion back and forth about the mounting point) and full rotational motion about the mounting point, classified as unstable motion in this study. The point that divides the two types of motion is called the separatrix. Because of the periodic nature of the restoring force on the pendulum, the pattern is repeated at every multiple of 360 deg. This results in multiple stable and unstable equilibrium points all divided by the separatrix. Various energies for the simple swinging pendulum results in the phase plot shown in Fig. 7.

Of primary concern in this study is the comparison of the two measures of determining stability and instability in the time and phase domains.

As already discussed, when the third body crosses the line of syzygies in the time domain, it is considered unstable. That is, it has unstable tendencies as it continues on is journey beyond the line of syzygies in an unstable fashion. Therefore, only initial third-body velocities away from L_4 not resulting in the third body crossing the line of syzygies are labeled stable. The trajectory resulting from this maximum initial velocity permitted (edge of the boundary envelope) is compared to the trajectory that defines the separatrix in the phase-space representation.

Comparison of Time-Domain vs Phase-Space-Domain Stability Criteria

First, the maximum initial velocity of the third body starting at the L_4 point and applied in the direction of $\theta = 106$ deg is determined for the boundary envelope above. As discussed earlier, $\theta = 106$ deg is selected for no special reason except that it is one of the highest kinetic-type energies permitted from L_4. It allows one of the largest velocities to emanate from L_4 without crossing the x axis within the 5,000,000 time units. The maximum allowed velocity in the 106-deg direction for the Jupiter–sun system is found to be 0.499244 dimensionless units. Data from other points surrounding L_4 also display similar results and are discussed later.

Figure 8 shows the Poincaré surface of section mapping found for the Jupiter–sun system ($\mu = 0.000953875$), $\theta = 106$ deg, and various dimensionless velocities originating from L_4 ranging from 0.4992 to 0.509126. In Fig. 8, there appears to be a stable cycle of six elliptic points. Around these six points appears a chain or necklace of six islands, each containing a set of invariant curves surrounding one of the fixed stable points. When Fig. 8 is observed, there are apparently three distinct types of motion displayed in this Jupiter–sun mapping: regular motion on invariant curves around the fixed points of stable periodic motion (elliptic points), chaotic motion bounded within regions of finite area around unstable periodic orbits, and unbounded escaping motion. Notice how the regions of regular and chaotic motion are mixed together where chains of islands are repeated on ever decreasing scales. Also notice how the hyperbolic points appear to be joined by a separatrix that is created using a velocity of 0.49962 dimensionless units. Again, according to the fundamental description of the various curves in the phase plane, the separatrix divides the stable from the unstable motion.

Note from Fig. 8 that dimensionless velocities with values less than the separatrix velocity of 0.49962 allow stable motion. Although not shown well in Fig. 8, one may also notice that for the values of 0.503 and 0.509125 the motion starts to become more

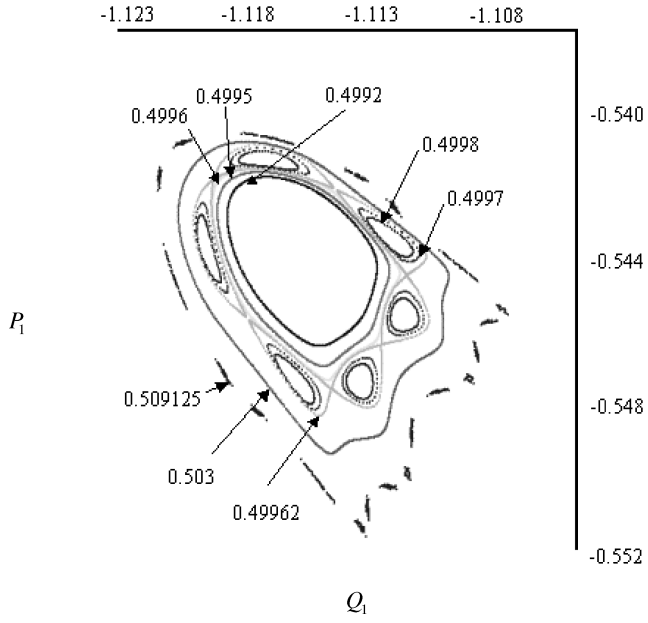

Fig. 8 Surface of section for the Jupiter–sun system, $\mu = 0.000953875$ and $\theta = 106$ deg.

Table 1 Various data points compared

Direction from L_4, deg	Maximum time-domain velocity	Maximum phase-space-domain velocity	% Difference	Difference in dimensional units, m/s
104.7	0.52488	0.53293	−1.53	−105.23654
106.0	0.49924	0.49962	−0.08	−4.96652
211.3	0.02214	0.02214	0.00	−0.01307
305.4	0.18244	0.18244	0.00	0.09149

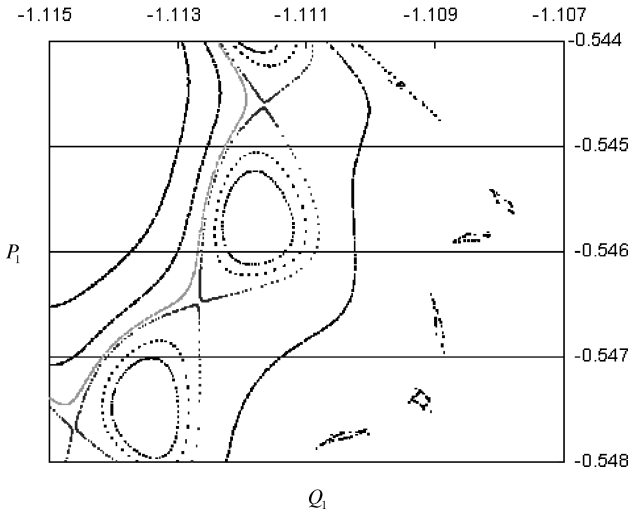

Fig. 9 Closeup of surface of section shown in Fig. 8.

chaotic. This is better shown in Fig. 9, which is a magnified portion of Fig. 8.

According to the Newtonian time-domain analysis, a maximum dimensionless value permitted for the velocity in the $\theta = 106$ deg direction is 0.499244. We assume that the third-body velocity that created the separatrix in the Fig. 9 phase-space plot is the maximum allowable for stable motion to take place. Under this assumption, the difference in the maximum phase-space (surface-of-section) velocity value (the velocity that created the separatrix) and the time-domain maximum velocity value (found from the boundary value envelop discussed earlier) is equal to $0.49962 - 0.49924 = 0.00037$ dimensionless time units. This is approximately a 0.074% difference in value and is equivalent to a difference of 4.84 m/s in the physical world, resulting in a very close agreement indeed.

Other points are also investigated and results show similar characteristics. Table 1 lists the data of all of the points investigated. Table 1 shows that the greatest difference found between the time-domain analysis and phase-space-domain analysis for maximum allowed velocities permitting stable motion is a 1.53% difference found in the 104.7-deg direction. This relates to a maximum of 105.24 m/s dimensional unit difference between the two measures of stability. A more in-depth investigation into the reason for this close resemblance is currently underway but results appear to support the validity of the noncrossing of the x axis as a threshold to determine stability in the Newtonian time domain.

Conclusions

With the use of the model of the circular restricted problem of three bodies, the stability of the third-body motion is investigated using the line of syzygies (x axis) as a boundary of stability. In an effort to verify the criterion of using the x axis as a measure or bound for stability, Poincaré's surfaces of sections are generated in the phase space to compare the regions of periodic, quasi-periodic, and stochastic motion around the stability of the Jupiter–sun system. Particular attention is directed to the two methods or measures that divide stable from unstable in the two time and phase domains, the line of syzygies, and the separatrix, respectfully. This study shows that there is an apparent correlation in the two methods used in the determination of stability of the third body that results in a maximum of 1.53% difference between the two methods for the data investigated. It is shown that using the x axis as a measure of stability in the Newtonian time domain and using the phase space surface of section results in close agreement.

References

[1]Hénon, M., "Numerical Study of Quadratic Area-Preserving Mappings," *Quarterly of Applied Mathmatics*, Vol. 27, No. 3, 1969, pp. 291–312.

[2]Hénon, M., "Numerical Exploration of the Restricted Problem VI. Hill's Case: Non-Periodic Orbits," *Astronomy and Astrophysics*, Vol. 9, No. 1, 1970, pp. 24–36.

[3]Hénon, M., and Heiles, C., "The Applicability of the Third Integral of Motion: Some Numerical Experiments," *Astronomical Journal*, Vol. 69, No. 1, 1964, pp. 73–79.

[4]Poincaré, H., *Les méthods nouvelles de la méchanique céleste*, Dover, New York, 1957.

[5]Alfriend, K., "The Stability of the Triangular Libration Points for Commensurability of Order Two," *Celestial Mechanics*, Vol. 1, 1970, pp. 351–359.

[6]Deprit, A., "Motion in the Vicinity of the Triangular Libration Centers," *Space Mathematics*, Pt. 2, Vol. 6, American Mathematical Society, Providence, RI, 1996, pp. 1–31.

[7]Henrard, J., "Concerning the Genealogy of Long Period Families at L_4," *Astronomy and Astrophysics*, Vol. 5, 1970, pp. 45–52.

[8]Pederson, P., "On the Periodic Orbits in the Neighborhood of the Triangular Equilibrium Points in the Restricted Problem of Three Bodies," *Monthly Notices of the Royal Astronomical Society*, Vol. 94, 1934, pp. 167–185.

[9]Szebehely, V., *Theory of Orbits*, Academic Press, New York, 1967, pp. 16–22.

[10]Tuckness, D. G., "Position and Velocity Sensitivities at the Triangular Libration Points," *Celestial Mechanics*, Vol. 61, 1995, pp. 1–19.

[11]McKenzie, R., and Szebehely, V., "Non-Linear Stability around the Triangular Libration Points," *Celestial Mechanics*, Vol. 23, 1981, pp. 223–229.